CeO 2 T CuO x Interactions and the Controlled Assembly of CeO 2 (111) and CeO 2 (100) Nanoparticles on an Oxidized Cu(111) Substrate

7 AUTHORS, INCLUDING:

Fan Yang
Chinese Academy of Sciences
33 PUBLICATIONS **693** CITATIONS

SEE PROFILE

Ping Liu
Brookhaven National Laboratory
118 PUBLICATIONS **4,192** CITATIONS

SEE PROFILE

Dario Stacchiola
Brookhaven National Laboratory
134 PUBLICATIONS **2,891** CITATIONS

SEE PROFILE

Jan Hrbek
Brookhaven National Laboratory
**213** PUBLICATIONS **6,016** CITATIONS

SEE PROFILE

CeO$_2$ ↔ CuO$_x$ Interactions and the Controlled Assembly of CeO$_2$(111) and CeO$_2$(100) Nanoparticles on an Oxidized Cu(111) Substrate

Fan Yang, YongMan Choi, Stefano Agnoli, Ping Liu, Dario Stacchiola, Jan Hrbek, and José A. Rodriguez*

Chemistry Department, Brookhaven National Laboratory, Upton, New York 11973, United States

ABSTRACT: The catalytic performance of ceria-based heterogeneous catalysts in many chemical transformations (water—gas shift reaction, CO oxidation, alcohol synthesis from CO/CO$_2$ hydrogenation, etc.) is affected by the surface structure of the ceria. To control the performance of ceria-containing inverse catalysts, we devised a method to grow ceria nanoparticles (NPs) exposing exclusively either (111) or (100) surfaces and characterized their surface structures by scanning tunneling microscopy. When cerium is vapor-deposited on Cu(111) in a background of molecular O$_2$, only CeO$_2$(111) NPs grow. However, if the surface of Cu(111) is preoxidized with O$_2$ or NO$_2$ to form a rectangular copper oxide phase, probably Cu$_4$O$_3$(001), CeO$_2$(100) NPs grow on the oxide template instead. These experimental findings are interpreted using results of density functional calculations. The (100) surface of bulk ceria reconstructs to preserve charge neutrality. This is not necessary for CeO$_2$(100) NPs grown on Cu$_4$O$_3$(001), where the topmost oxygen layer of Cu$_4$O$_3$ is shared with the interfacial layer of cerium. After the CeO$_2$(100)/CuO$_x$/Cu(111) surfaces were exposed to CO, the copper oxide was reduced but the shape of the CeO$_2$(100) NPs remained intact. This opens the door for diverse applications in catalysis.
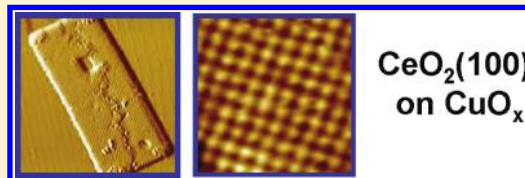
INTRODUCTION

Interest in oxide NPs supported on a metal surface has grown substantially in recent years,[1−5] in part due to their unique reactivity and selectivity in catalysis. Cerium oxides supported on copper are an excellent example to showcase the catalytic properties of supported oxide NPs.[6−10] Copper and cerium oxides are cost-effective materials widely used in catalytic applications. These two materials individually are not good catalysts for reactions such as CO oxidation or the water—gas shift (WGS). Our recent studies have shown that when ceria NPs are supported on Cu(111), this inverse model catalyst becomes very active for CO oxidation[6] and the WGS.[7] Meanwhile, newly designed inverse CeO$_x$/CuO$_x$ powder nanocatalysts display a very high activity for the preferential oxidation of CO (PROX).[8]

To control the performance of ceria-containing inverse catalysts, we developed a new methodology that leads to the growth of ceria NPs which expose exclusively the (111) or (100) surface planes. Previously, (111)-terminated CeO$_2$ NPs were successfully synthesized and characterized on Cu(111).[6,9,10] However, the (100) plane of CeO$_2$ is the least stable one and inherently the most reactive surface among the low index planes of ceria.[11,12] Due to its polar character, the (100)-terminated ceria is intrinsically unstable and prone to reconstruction, imposing challenges for the synthesis of CeO$_2$(100) NPs. So far, progress has been made in the liquid-phase synthesis of ceria polyhedral NPs[13,14] or quasi-2D nanosheets,[15] which expose mostly (100) planes but also contain (111) and (110) planes. A problem is that catalysts prepared by the liquid-phase synthesis are difficult to characterize, especially regarding their surface structure and properties, which are essential for the understanding of active sites in catalysis.

In this paper, we report a method to grow crystalline CeO$_2$(100) NPs under ultrahigh vacuum (UHV) conditions and characterize their surface structures using scanning tunneling microscopy (STM).

EXPERIMENTAL AND COMPUTATIONAL METHODS

STM studies were conducted in a commercial Omicron variable-temperature STM system, equipped with surface cleaning facilities and an e-beam metal evaporator.[16] The base pressure of the STM chamber was <1 × 10^{-10} mbar. The sample temperature was measured by a K-type thermocouple, which was installed on a linear motion feedthrough and pressed against the top of the sample surface. A resistive heater posited at the back of the sample could increase the sample temperature to 1000 K. Chemically etched W tips were used for imaging the surface. SPIP software (Image Metrology, Denmark) was used to process and analyze STM images. The Cu(111) single crystal was pretreated in a mixed H$_2$/Ar flow at 500 °C to remove any possible sulfur impurities from the bulk. After being transferred into UHV, the sample was cleaned by repeated cycles of Ar sputtering (1 keV, 40 min) and annealing (900 K, 10 min). CO gas was cleaned using a trap of liquid N$_2$ prior to the reduction of the Cu$_2$O surface. Ce atoms were evaporated by e-beam heating Ce foils (>99.9% purity, Alfa) housed in a Ta crucible.[6]

Periodic density functional theory (DFT) calculations were conducted using the Vienna ab initio simulation package (VASP)[17,18] with projector augmented wave (PAW)[19] potentials and the
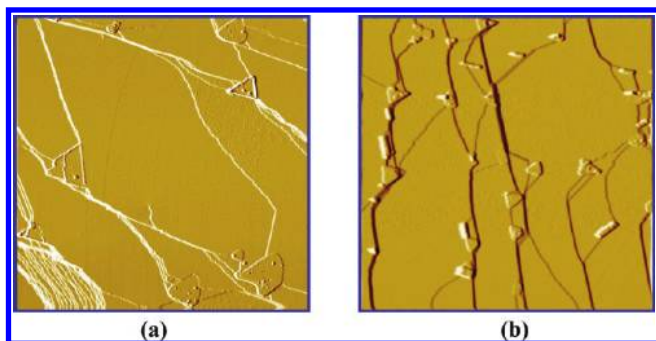
Figure 1. STM images of supported CeO_2 NPs prepared by Ce deposition in 5×10^{-7} mbar of O_2 at (a) 650 K and (b) 500 K, followed by annealing in 5×10^{-7} mbar of O_2 at 650 K. Both images are shown in the derivative mode. Image sizes are 500×500 nm^2.

Perdew–Wang (PW91)[20] exchange-correlation functional. All calculations were carried out with a 400 eV kinetic energy cutoff for a plane wave basis set. Monkhorst–Pack[21] meshes with $(3 \times 3 \times 3)$ and $(3 \times 3 \times 1)$ k-points were utilized for bulk and surface calculations, respectively. The flat Cu(111) surface $(a_0 = 3.634$ Å$)$ was simulated by a four-layer p(3×3) slab model with a vacuum space of 20 Å, and one CeO_2-like O–Ce–O layer (four Ce ions and eight O ions) was deposited on Cu(111) to model CeO_2/Cu(111). Cu_4O_3 has a $I4_1/amd$ structure with lattice parameters of $a = b = 5.875$ Å and $c = 9.860$ Å, which are in good agreement with the experimental values $(a = b = 5.822$ Å and $c = 9.844$ Å$)$.[22] The Cu_4O_3(001) surface was simulated by an eight-layer p(1×1) slab model with a vacuum space of 20 Å, and one CeO_2-like O–Ce–O layer (two Ce ions and four O ions) was deposited on Cu_4O_3(001) to model CeO_2/Cu(111). In addition, to estimate the lattice mismatch of the CeO_2-like structure on Cu(111) and Cu_4O_3(001), we also optimized bulk CeO_2 $(a_0 = 5.451$ Å$)$. For surface calculations, the bottom two and four layers of the Cu and Cu_4O_3 surfaces, respectively, were fixed at the lattice position, while the other atoms, including the CeO_2-like surface, were fully relaxed. The formation energy of the CeO_2-like strucure is calculated according to $E_f = E[CeO_2/surf] - nE[Ce] - 2nE[O_2]/2 - E[surf]$, where $E[CeO_2/surf]$, $E[Ce]$, $E[O_2]$, and $E[surf]$ are the energies of a deposited CeO_2-like structure on a surface, the Ce atom, oxygen in the triplet state, and a surface (Cu(111) or Cu_4O_3(001)) and n as the number of Ce atoms. Similar to the previous study,[23] the energy of the Ce atom was obtained from its bulk structure. Spin polarization calculations were used, and DFT + U with U_{eff} = 4.5 eV for Ce[7] was utilized.

■ RESULTS AND DISCUSSION

Figure 1a shows ceria NPs exposing the highly stable (111) surface plane which were synthesized via the evaporation of Ce atoms in 5×10^{-7} mbar of O_2 onto the Cu(111) surface held at 650 K. According to X-ray photoelectron spectroscopy (XPS) measurements, the as-grown ceria NPs are fully oxidized[6] and exhibit overlapping moiré patterns due to the oxidation of Cu(111) and the formation of an interfacial Cu_2O(111)-like layer between Cu(111) and CeO_2(111).[6,16] Interaction of CO with the CeO_2/Cu_2O sample at temperatures above 650K leads to its reduction and a loss of moiré patterns.[6] Two types of ceria NPs were observed to grow on the copper surface when the growth temperature was lowered to ~500 K and annealed at

650 K in O_2. As Figure 1b shows the ceria NPs exhibit two shapes: triangular and rectangular. The triangular-shaped ceria (t-ceria) islands display the (111) surface structure, whereas the rectangular-shaped ceria NPs (r-ceria) exhibit a square lattice. The growth of t-ceria NPs is anticipated since (a) the (111) face is the most stable surface of CeO_2 and (b) the hexagonal symmetry of CeO_2(111) is matched by those of Cu(111) and Cu_2O(111). Is the r-ceria a metastable phase appearing at intermediate temperatures? The surface of Figure 1b was further annealed at higher temperatures (650–750 K). Neither a shape change nor a structural transition of r-ceria NPs was observed, ruling out the possibility of r-ceria being a kinetically trapped phase. Furthermore, XPS showed that the Ce atoms in these structures were fully oxidized.

The growth of crystalline NPs on a single crystal surface depends on many parameters, including the lattice mismatch, crystal orientation, growth temperature, and interfacial energy. A surface with domains of different symmetries should direct the growth of NPs to different interfacial structures. The oxidized Cu(111) surface can provide such a substrate. Surface oxidation of Cu(111) using molecular O_2 under vacuum conditions $(10^{-8}-10^{-6}$ mbar) leads to the formation of the so-called "44" and "29" structures[24] of a Cu_2O(111)-like oxide monolayer. As described in our recent paper,[6] supported ceria NPs can dissociate O_2, with atomic oxygen spilling over to the Cu(111) substrate and forming different copper oxide domains whose structure is dependent on the distance from the ceria NP. The presence of ceria NPs promotes the oxidation of Cu(111) beyond the 44 and 29 surface oxides and leads to the formation of a novel 3D phase of copper oxide with a rectangular unit cell.[6] The novel oxide phase, termed a rectangular copper oxide, has a symmetry matching that of r-ceria and might serve as the substrate for the growth of r-ceria NPs.

Is the growth of r-ceria NPs solely a consequence of the formation of a rectangular copper oxide template? To test this hypothesis, we attempted to grow exclusively r-ceria NPs. First, the 44-Cu_2O surface oxide was formed by oxidizing the Cu(111) substrate in 5×10^{-7} mbar of O_2 at 550 K.[25] Next, ceria clusters were deposited on the surface of the 44-Cu_2O surface oxide at room temperature, as shown by Figure 2a. The as-deposited ceria clusters are dispersed on the Cu_2O surface with a narrow size distribution (0.6–2.0 nm in radius). At temperatures below 550 K, ceria clusters have limited mobility on the Cu_2O surface oxide and do not sinter. The surface was then annealed in 5×10^{-7} mbar of O_2 at 400, 450, 500, and 550 K and held for 10 min at each temperature. Parts b and c of Figure 2 show the results of the sequential annealing steps. The rows of copper oxide are decorated by small ceria clusters and form domains rotated by 45° or 90°; in contrast, the 44-Cu_2O surface oxide domains are rotated 60° or 120°. Parts b and c of Figure 2 also illustrate that the continuing surface oxidation is accompanied by shrinking of ceria clusters. These ceria clusters start to sinter at temperature above 650 K. After annealing to 750 K, most ceria clusters move to step edges, forming r-ceria NPs (Figure 2d).

The structure and morphology of r-ceria NPs are displayed in Figure 3. The apparent heights of the r-ceria NPs are measured as multiples of ~0.30 nm. Shown in Figure 3a is a multilayer r-ceria NP with a lattice spacing of 0.56 nm. Such lattice spacing is observed for all multilayer r-ceria NPs (>20 NPs were examined). Ceria NPs of monolayer thickness (~0.30 nm) have a smaller square lattice of 0.40 nm that could be observed under aggressive scanning conditions (i.e., <1.0 V sample bias, Figure 3b). The apparent height and the square lattice with 0.40 nm spacing
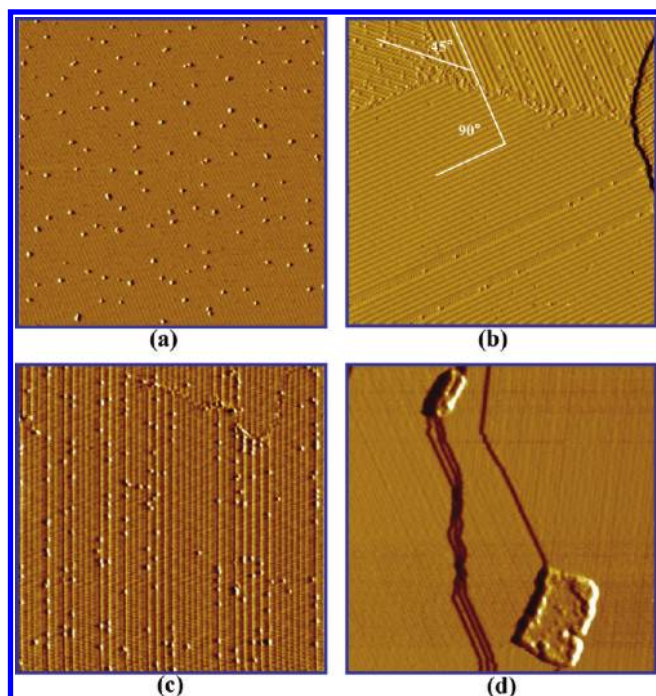
Figure 4. STM images of $CeO_2(100)$ NPs prepared by Ce deposition in 5×10^{-7} mbar of O_2 at 650 K on a copper oxide surface, formed by oxidizing Cu(111) with NO_2 at 600 K. Both large-scale images are shown in the derivative mode. Image sizes are (a) 500×500 nm^2 and (b) 40×40 nm^2.

Figure 2. STM images for the synthesis of rectangular-shaped ceria NPs on Cu(111): (a) ceria grown by evaporating cerium in 5×10^{-7} mbar of O_2 at 300 K onto a 44-Cu_2O surface oxide, which was formed by oxidizing the Cu(111) substrate in 5×10^{-7} mbar of O_2 at 550 K; (b, c) surface of (a) after being heated in 5×10^{-7} mbar of O_2 at 400, 450, 500, and 550 K for 10 min, respectively; (d) surface of (c) after being annealed in 5×10^{-7} mbar of O_2 at 750 K for 10 min. All images are shown in the derivative mode to enhance the contrast of surface features. Image sizes are (a, d) 200×200 nm^2 and (b, c) 100×100 nm^2.
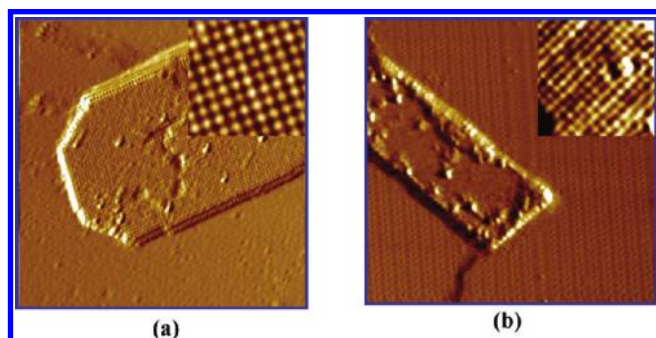

Figure 3. STM images of the structure of the rectangular-shaped ceria NPs. The atomic structure of each ceria NP is zoomed in the inset. Both large-scale images are shown in the derivative mode. Image sizes are (a) 50×50 nm^2 and (b) 40×40 nm^2. Both insets are 5×5 nm^2. Scanning conditions are (a) $V_s = 1.6$ V and $I_t = 0.1$ nA (same for the inset) and (b) $V_s = 1.0$ V and $I_t = 0.1$ nA (inset: $V_s = 0.8$ V, $I_t = 0.1$ nA).

oxidation of Cu(111) by using atomic oxygen sources.[26] In our study, we used NO_2 to induce the rectangular copper oxide growth on Cu(111). After a dose of 11 L of NO_2 at 600 K, the rectangular copper oxide phase was formed on the Cu(111) surface. Subsequently, ceria NPs were grown on the rectangular copper oxide surface by evaporating Ce atoms in 5×10^{-7} mbar of O_2 at 650 K. As shown in Figure 4, all ceria NPs are rectangular-shaped (Figure 4a) and the ceria NP exhibits a square lattice with a lattice spacing of 0.56 nm (Figure 4b). Note that both types of ceria NPs, $CeO_2(111)$ and $CeO_2(100)$, exhibit two kinds of edges, one with higher brightness than the NP surface (see Figures 1a and 3b) and the other with the same brightness as the NP surface (see Figures 1a and 4b). A similar phenomenon was seen on MoS_2 NPs and interpreted as the presence of the metallic brim states.[27]

The structural details of the rectangular copper oxide cannot be resolved using solely STM data. Both XPS and STM studies suggest the rectangular copper oxide has a higher oxygen concentration than the Cu_2O surface oxide. Our previous study[28] has shown the presence of an intermediate phase, Cu_4O_3, during the phase transition between Cu_2O and CuO. The (001) surface of Cu_4O_3, which is thermodynamically favorable, exhibits a pseudo square lattice and could serve as the substrate for the growth of $CeO_2(100)$. Here, we assume the observed rectangular copper oxide phase originates from the $Cu_4O_3(001)$ layers, which could be distorted on Cu(111) due to the interfacial strain and exhibit a rectangular unit cell larger than that of the unsupported $Cu_4O_3(001)$.

We used DFT calculations to gain insight into the formation of r-ceria. To reduce the computational load, the (001)-terminated bulk Cu_4O_3, instead of Cu(111)-supported $Cu_4O_3(001)$ layers, was used to build a CeO_2 layer in our DFT calculations. The structure of CeO_2 on Cu(111) was also computed as a comparison. Figure 5 displays the optimized geometries of stoichiometric CeO_2 deposited on Cu(111) and $Cu_4O_3(001)$. Our calculations show that $Cu_4O_3(001)$ allows the growth of $CeO_2(100)$, while on Cu(111), $CeO_2(111)$ is the most stable structure. The formation energy of $CeO_2(111)$ on Cu(111) is -10.8 J/m^2, slightly lower than that of $CeO_2(100)$ on $Cu_4O_3(001)$, -8.9 J/m^2. Therefore, the growth of $CeO_2(100)$ on $Cu_4O_3(001)$ is thermodynamically favorable and has a stability comparable to that of $CeO_2(111)/Cu(111)$.

Our calculations also show, unlike the growth of CeO_2 on Cu(111), CeO_2 grows as a pseudomorphic layer on

closely match those of the unreconstructed $CeO_2(100)$ surface. Therefore, we assign the r-ceria NPs as $CeO_2(100)$ NPs. The 0.56 nm spacing observed in the STM images of multilayer r-ceria NPs might be due to the surface relaxation and will be discussed later.

We have demonstrated that ceria-promoted copper oxidation and the formation of rectangular copper oxides are the key to the formation of $CeO_2(100)$ NPs. For the purpose of the controlled synthesis of $CeO_2(100)$ NPs, a simpler strategy is to facilitate the

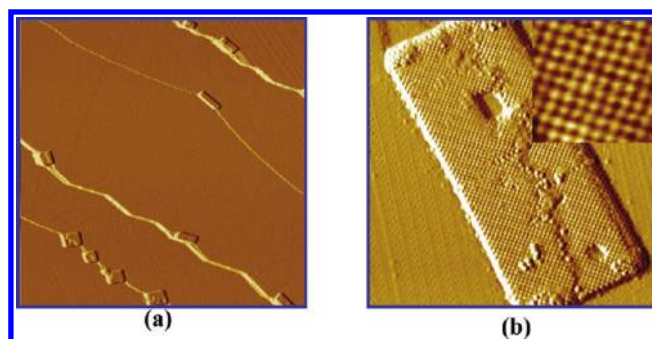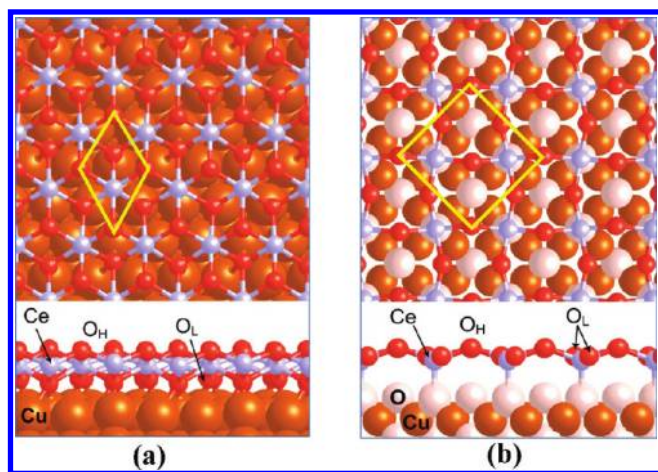**Figure 5.** Top and side views of DFT-optimized CeO_2 structures on (a) Cu(111) and (b) Cu_4O_3(001). The rhombus and rectangle in yellow represent unit cells. Ce and O atoms on CeO_2 are in light blue and in red, respectively, while Cu and O atoms on the substrates are in orange and in light pink, respectively.
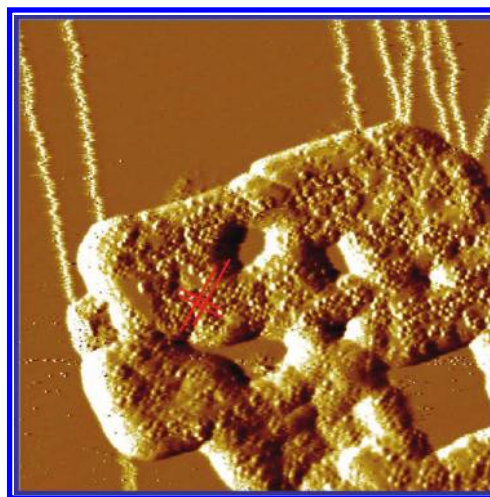

Figure 6. STM image of a sintered CeO_2(100) NP after CO reduction. The surface was obtained by reducing the surface of Figure 2d in 5×10^{-6} mbar of CO at 750 K for 2 h. The image size is 50×50 nm^2. The red lines mark the position of ceria clusters on the surface of the CeO_2(100) NP.

Cu_4O_3(001); i.e., the lattice of CeO_2(100) is expanded to adapt to the lattice of Cu_4O_3(001). The distance between nearest Ce cations of the relaxed CeO_2 layer on Cu_4O_3(001) is computed at 0.416 nm, 8.1% larger than that of bulk CeO_2 (0.385 nm). The strain introduced by the expansion of the CeO_2 lattice is relaxed through the lateral displacements of oxygen atoms in the CeO_2 layer, as shown in Figure 5b. In the case of the CeO_2(100) NPs, such a large expansion probably does not occur due to local relaxation. The lateral displacements of oxygen atoms are not obvious in our STM images. In STM, since the measurement was conducted at positive sample bias, the STM contrast presumably originates from the 4f states of Ce cations. Our STM measurement gives the Ce–Ce distance at 0.40 nm in the monolayer CeO_2(100), which also suggests some expansion of the CeO_2-(100) lattice. Thus, the difference in lattice parameters obtained from STM and DFT might be due to the fact that STM measurements are conducted on CeO_2(100) NPs while the calculation is performed with a full CeO_2(100) layer. For large coverages of ceria, we observed three-dimensional growth instead of a single full layer of CeO_2(100) wetting the underlying copper oxide.

In the case of multilayer CeO_2(100) NPs, the observed lattice spacing of 0.56 nm might be caused by a strong surface relaxation. Note that a previous STM study[29] on the bulk CeO_2(100) surface shows a variety of surface reconstructions. CeO_2, along the (001) direction, is stacked by alternating planes of cerium cations and oxygen anions. The charge density of the cerium plane equals that of the oxygen plane (but with opposite sign). A nonzero charge dipole persists for CeO_2(100) when the bulk is terminated by oxygen at both sides of the slab. Consequently, the surface of CeO_2(100) reconstructs to preserve charge neutrality. In CeO_2(100) NPs grown on Cu_4O_3(001), the topmost oxygen layer of Cu_4O_3 is shared with the interfacial layer of cerium. In the case of the CeO_2(100) monolayer, the added layer of cerium is even with the layer of oxygen and charges cancel out at the surface. Therefore, the surface relaxation of a CeO_2(100) monolayer on Cu_4O_3(001) is minimal compared with that of multilayer/bulk CeO_2(100). As the surface electrostatic potential increases with the thickness of the CeO_2(100) oxide film,[3] we

expect the surface relaxation of multilayer CeO_2(100) NPs is more severe and might involve the displacements of top-layer Ce atoms. Within this hypothesis, the 0.56 nm square lattice observed in STM could suggest a $(\sqrt{2} \times \sqrt{2})$ reconstruction of Ce cations in the top layer. In other words, Ce atoms are relaxed vertically in such a way that only half of the surface Ce atoms are resolved in STM.

The removal of the Cu_4O_3(001) substrate could destabilize the surface of CeO_2(100). We used the sample of CeO_2(100) NPs prepared in Figure 2 and reduced it in 5×10^{-6} mbar of CO at 750 K for 2 h to fully remove the copper oxides present on Cu(111).[16] Figure 6 shows that the CeO_2(100) NPs agglomerate and form large rectangular particles. The ripened CeO_2 NP displays a roughened surface, which in part might be due to the presumed absence of an interfacial copper oxide layer that otherwise stabilizes CeO_2(100). Also some oxygen could be removed from ceria according to XPS measurements. Figure 6 also shows that small clusters at the surface of the ripened NP remain ordered in a square lattice, as marked by red lines. The lattice of clusters have a spacing of $\sim$0.5–0.6 nm, matching the lattice periodicity observed on multilayer CeO_2(100) NPs and suggesting that the crystal structure and orientation of CeO_2-(100) NPs remain intact after CO reduction. Note that the reduction kinetics of surface copper oxides is highly dependent on the oxidation conditions used to prepare the CeO_2(100) NPs. We also tried to reduce the sample of CeO_2(100) NPs prepared in Figure 3. Using the same conditions, i.e., in 5×10^{-6} mbar of CO at 750 K for 2 h, the surface of CeO_2(100) NPs remained unchanged, except for a few vacancies observed in the surface of rectangular copper oxides.

■ SUMMARY AND CONCLUSIONS

In conclusion, we have described preparation procedures on how to grow exclusively either CeO_2(111) or CeO_2(100) NPs on Cu(111), providing a better way to control the performance of ceria-containing inverse catalysts. In traditional approaches for growing oxides on a metal surface, the goal is to have initially a metal substrate that is chemically inert and thermally stable.[3] Our

study, on the other hand, illustrates that a reactive substrate provides the opportunity and versatility for the controlled synthesis of multiple facets and the growth of less stable/more reactive NPs. The growth of $CeO_2(100)$ NPs is induced by the formation of a rectangular copper oxide phase on $Cu(111)$. In contact with the rectangular copper oxide face, presumably $Cu_4O_3(001)$, Ce atoms are constrained in a square configuration and forced to adopt a geometry that is not stable as a termination for bulk ceria. DFT calculations show that the formation energy of $CeO_2(111)$ on $Cu(111)$ is -10.8 J/m^2, slightly lower than that of CeO_2-(100) on $Cu_4O_3(001)$, -8.9 J/m^2. The growth of $CeO_2(100)$ on $Cu_4O_3(001)$ is thermodynamically favorable and has a stability comparable to that of $CeO_2(111)/Cu(111)$. Upon reduction of the underlying copper oxide, the shape of the $CeO_2(100)$ NPs did not change. The controlled growth of $CeO_2(100)$ NPs opens the door for enhanced chemical activity and applications in important processes (CO oxidation, PROX, WGS, synthesis of alcohols from CO/CO_2 hydrogenation, NO reduction, etc.) catalyzed by copper—ceria catalysts.

■ AUTHOR INFORMATION

Corresponding Author
*E-mail: rodrigez@bnl.gov.

■ ACKNOWLEDGMENT

■ REFERENCES

(1) Rodriguez, J. A.; Ma, S.; Liu, P.; Hrbek, J.; Evans, J.; Perez, M. *Science* **2007**, *318*, 1757–1760.

(2) Freund, H. J.; Pacchioni, G. *Chem. Soc. Rev.* **2008**, *37*, 2224–2242.

(3) Nilius, N. *Surf. Sci. Rep.* **2009**, *64*, 595–659.

(4) Rodriguez, J. A.; Hrbek, J. *Surf. Sci.* **2010**, *604*, 241–244.

(5) Netzer, F. P.; Allegretti, F.; Surnev, S. *J. Vac. Sci. Technol., B* **2010**, *28*, 1–16.

(6) Yang, F.; Graciani, J.; Evans, J.; Liu, P.; Hrbek, J.; Sanz, J. F.; Rodriguez, J. A. *J. Am. Chem. Soc.* **2011**, *133*, 3444–3451.

(7) Rodriguez, J. A.; Graciani, J.; Evans, J.; Park, J. B.; Yang, F.; Stacchiola, D.; Senanayake, S. D.; Ma, S. G.; Perez, M.; Liu, P.; Sanz, J. F.; Hrbek, J. *Angew. Chem., Int. Ed.* **2009**, *48*, 8047–8050.

(8) Hornes, A.; Hungria, A. B.; Bera, P.; Camara, A. L.; Fernandez-Garcia, M.; Martinez-Arias, A.; Barrio, L.; Estrella, M.; Zhou, G.; Fonseca, J. J.; Hanson, J. C.; Rodriguez, J. A. *J. Am. Chem. Soc.* **2010**, *132*, 34–36.

(9) Dvorak, F.; Stetsovych, O.; Steger, M.; Cherradi, E.; Matolinova, I.; Tsud, N.; Skoda, M.; Skala, T.; Myslivecek, J.; Matolin, V. *J. Phys. Chem. C* **2011**, *115*, 7496–7503.

(10) Wrobel, R.; Suchorski, Y.; Becker, S.; Weiss, H. *Surf. Sci.* **2008**, *602*, 436–442.

(11) Baudin, M.; Wójcik, M.; Hermansson, K. *Surf. Sci.* **2000**, *468*, 51–61.

(12) Nolan, M.; Grigoleit, S.; Sayle, D. C.; Parker, S. C.; Watson, G. W. *Surf. Sci.* **2005**, *576*, 217–229.

(13) Mai, H.-X.; Sun, L.-D.; Zhang, Y.-W.; Si, R.; Feng, W.; Zhang, H.-P.; Liu, H.-C.; Yan, C.-H. *J. Phys. Chem. B* **2005**, *109*, 24380–24385.

(14) Si, R.; Flytzani-Stephanopoulos, M. *Angew. Chem., Int. Ed.* **2008**, *47*, 2884–2887.

(15) Wang, D.; Kang, Y.; Doan-Nguyen, V.; Chen, J.; Küngas, R.; Wieder, N. L.; Bakhmutsky, K.; Gorte, R. J.; Murray, C. B. *Angew. Chem., Int. Ed.* **2011**, *50*, 4378–4381.

(16) Yang, F.; Choi, Y.; Liu, P.; Hrbek, J.; Rodriguez, J. A. *J. Phys. Chem. C* **2010**, *114*, 17042–17050.

(17) Kresse, G.; Hafner, J. *Phys. Rev. B* **1993**, *47*, 558–561.

(18) Kresse, G.; Furthmuller, J. *Phys. Rev. B* **1996**, *54*, 11169–11186.

(19) Blöchl, P. E. *Phys. Rev. B* **1994**, *50*, 17953–17979.

(20) Perdew, J. P.; Wang, Y. *Phys. Rev. B* **1992**, *45*, 13244–13249.

(21) Monkhorst, H. J.; Pack, J. D. *Phys. Rev. B* **1976**, *13*, 5188–5192.

(22) Pinsard-Gaudart, L.; Rodríguez-Carvajal, J.; Gukasov, A.; Monod, P. *Phys. Rev. B* **2004**, *69*, 104408–9.

(23) Loschen, C.; Carrasco, J.; Neyman, K. M.; Illas, F. *Phys. Rev. B* **2007**, *75*, 035115–8.

(24) Jensen, F.; Besenbacher, F.; Laegsgaard, E.; Stensgaard, I. *Surf. Sci.* **1991**, *259*, L774–L780.

(25) Yang, F.; Choi, Y.; Liu, P.; Stacchiola, D.; Hrbek, J.; Rodriguez, J. A. *J. Am. Chem. Soc.* **2011**, *133*, 11474–11477.

(26) Malik, I. J.; Hrbek, J. *J. Phys. Chem.* **1991**, *95*, 10188–10190.

(27) Bollinger, M. V.; Lauritsen, J. V.; Jacobsen, K. W.; Norskov, J. K.; Helveg, S.; Besenbacher, F. *Phys. Rev. Lett.* **2001**, *87*, 196803–4.

(28) Wang, X. Q.; Hanson, J. C.; Frenkel, A. I.; Kim, J. Y.; Rodriguez, J. A. *J. Phys. Chem. B* **2004**, *108*, 13667–13673.

(29) Nörenberg, H.; Harding, J. H. *Surf. Sci.* **2001**, *477*, 17–24.

23066

dx.doi.org/10.1021/jp2082837 |*J. Phys. Chem. C* 2011, 115, 23062–23066